Pharm Res (2012) 29:1670–1688
DOI 10.1007/s11095-012-0691-y

RESEARCH PAPER

Comparing MDI and DPI Aerosol Deposition Using *In Vitro* Experiments and a New Stochastic Individual Path (SIP) Model of the Conducting Airways

P. Worth Longest • Geng Tian • Ross L. Walenga • Michael Hindle

Received: 21 October 2011 / Accepted: 19 January 2012 / Published online: 31 January 2012

ABSTRACT

Purpose Deposition characteristics of MDI and DPI aerosols were compared throughout the conducting airways for the first time using a combination of *in vitro* experiments and a newly developed stochastic individual path (SIP) model for different inhalation profiles.

Methods *In vitro* experiments were used to determine initial particle distribution profiles and to validate computational fluid dynamics (CFD) model results for a MDI and DPI delivering the same dose of drug in a geometry of the mouth-throat and tracheobronchial airways. The validated CFD model was then used to predict the transport and deposition of the drug using correct and incorrect inhalation profiles for each inhaler.

Results The MDI delivered approximately two times more drug to the tracheobronchial region compared with the DPI for both correct and incorrect inhalation profiles. Errors in inhalation reduced the deposited tracheobronchial dose by approximately 30% for both inhalers. The DPI delivered the largest dose to the mouth-throat (~70%) and the MDI delivered the largest dose to the alveolar airways (~50%).

Conclusions The developed *in silico* model provides new insights into the lung delivery of pharmaceutical aerosols and can be applied in future studies in combination with pharmacokinetic analysis to establish bioequivalence between devices.

P. W. Longest (✉) • G. Tian • R. L. Walenga
Department of Mechanical Engineering
Virginia Commonwealth University
Richmond, Virginia, USA
e-mail: pwlongest@vcu.edu

P. W. Longest • M. Hindle
Department of Pharmaceutics, Virginia Commonwealth University
401 West Main Street, P.O. Box 843015, Richmond
Virginia 23284-3015, USA

KEY WORDS aerosol deposition · bioequivalence testing of inhalers · inhaler performance · respiratory drug delivery · stochastic lung modeling

ABBREVIATIONS

B#	bifurcation number (1 is trachea plus main bronchi)
C/P	central to peripheral lung deposition ratio
CFC	chlorofluorocarbon
CFD	computational fluid dynamics
COPD	chronic obstructive pulmonary disease
CT	computed tomography
DE	deposition efficiency
DF	deposition fraction
DPI	dry powder inhaler
ECG	enhanced condensational growth
exp	experiment
FR	fraction remaining
HFA	hydrofluoroalkane
HPLC	high-performance liquid chromatography
LRN	low Reynolds number
MDI	metered dose inhaler
MMAD	mass median aerodynamic diameter
MT	mouth-throat
NGI	next generation impactor
PF	penetration fraction
QD	quick and deep inhalation waveform
SD	slow and deep inhalation waveform
SIP	stochastic individual path
$T_{a\text{-}mean}$	time of mean accelerating flow
TB	tracheobronchial
USP	United States Pharmacopeial

INTRODUCTION

The two most common devices for respiratory drug delivery are currently metered dose inhalers (MDIs) and dry powder inhalers (DPIs). As reviewed by numerous other studies, each of these devices has inherent strengths and weaknesses (1–4). For example, MDIs require coordination between inhalation and activation that is difficult to achieve by many users (5,6). In contrast, most DPIs rely on a subject's inspiratory effort to aerosolize a powder and deliver the drug (4). As a result, the dose delivered by DPIs is reported to be more dependent on inhalation flow rate than with MDIs (7,8). Accurate comparisons of lung delivery and deposition for MDI and DPI devices have previously required radionuclide imaging or pharmacokinetic analysis in human subjects (4,9). Furthermore, previous studies have not compared the lung deposition of MDI and DPI aerosols for different inhalation flow conditions. Predictions of delivered dose and regional deposition characteristics for MDIs and DPIs are needed for a range of typical inhalation flow conditions in order to better compare the performance of these commonly used inhalers.

Radionuclide imaging and pharmacokinetic studies of MDI and DPI aerosol delivery in humans report a variety of outcomes. Pharmacokinetic studies have previously been used to establish the bioequivalence of newer DPIs with existing MDIs (10). Gamma scintigraphy studies have indicated improved lung delivery of typical DPIs compared to CFC-based MDIs (11), which is consistent with observations of improved clinical effects at lower doses (12,13). However, newer HFA-based MDIs often provide equivalent or improved lung delivery, especially when used with spacer devices, compared with DPIs (4,14). Imaging studies of MDI and DPI delivery also typically report high central lung deposition of the aerosol, expressed as a central to peripheral deposition ratio (C/P) above 1 (9). However, definitions of regional boundaries in the airways are often difficult to determine and differ among imaging studies (9).

Current radionuclide and pharmacokinetic studies that determine the dose and distribution of pharmaceutical aerosols in the lungs have a number of limitations. Both approaches require the use of human subjects and include either some radiation exposure (with imaging) or the collection of biological fluids (with pharmacokinetic analysis). Further limitations of imaging studies include the requirement to label the aerosols with a radionuclide and the need for attenuation correction factors (9). Significant efforts are required to label the MDI and DPI formulations without modifying the aerodynamic properties and to ensure there are no differences between the particle size distributions of the labeled and unlabeled aerosols. In contrast, pharmacokinetic studies do not require the use of radioactive labels such that the commercially available or clinical form of the aerosol and inhaler can be tested. However, this approach only provides an estimate of total lung deposition without information on where the aerosol deposits, i.e., C/P deposition ratios are not available. Recent studies have combined 3-D radionuclide imaging with CT scanning of the same subject to better interpret the deposition locations of aerosols in the respiratory anatomy (15). However, the reported CT resolution of these studies (~ 4.4 mm) is likely only capable of resolving the first few bronchi in the lungs. A numerical model capable of predicting delivery to the tracheobronchial (TB) airways or regions of these airways for pharmaceutical aerosols would clearly provide many benefits in comparison with existing imaging and pharmacokinetic methods.

Numerical models of aerosol transport and deposition in large regions of the lungs (e.g., the TB airways) typically consider monodisperse particles and often exclude the effects of the inhaler device (16). One-dimensional whole-lung deposition models implement algebraic correlations to account for deposition by various mechanisms and can effectively predict deposition down to the branch-averaged level (17–19). However, these models often neglect factors relevant to the delivery of pharmaceutical aerosols. Computational fluid dynamics (CFD) models of aerosol transport starting with the mouth have extended through the upper TB airways (20–23) and even lower TB airways (24,25). However, these models often neglect the effects of the inhaler and typically assume stable monodisperse particles and steady state flow fields (16). A number of studies have indicated that ambient monodisperse aerosols and pharmaceutical aerosols from spray devices and DPIs deposit very differently in the upper airways, which affects downstream transport and delivery (26,27). Factors affecting the deposition of pharmaceutical aerosols include turbulence from the inhaler (28,29), spray momentum (27,30), and inlet jet effects (31). DeHaan and Finlay (26) proposed correlations to account for the mouth deposition of aerosols from DPIs with small diameter inlets, and Finlay and Martin (32) showed that these correlations agreed well with experimental data for DPIs. Similar correlations do not currently exist for spray devices, such as MDIs and softmist inhalers.

Longest and colleagues recently reported a CFD-based stochastic individual path (SIP) modeling approach to predict the delivery of pharmaceutical aerosols throughout the TB airways (33,34). In this approach, aerosol transport and deposition are modeled from the inhaler through the mouth-throat and to the third respiratory bifurcation (B3) of an asymmetrical model. Thereafter, individual pathways are stochastically generated in which one branch of each bifurcation is continued and one is not. As a result, three dimensional stochastic paths are built to characterize deposition throughout the TB airways in a highly efficient manner. Tian *et al.* (33) used this modeling approach to characterize the

growth of pharmaceutical aerosols delivered with a newly proposed enhanced condensational growth (ECG) method (35). For a DPI, Tian *et al.* (34) showed that deposition in the upper airways through approximately B3 was affected by the use of a realistic transient inhalation waveform compared with a steady state approximation. In the SIP models starting with the fourth bifurcation, steady state approximations were highly accurate and one SIP geometry was found to sufficiently represent the deposition in an individual lobe of the lung. However, Tian *et al.* (34) only considered DPI delivery to a single lobe using the SIP approach.

Inhalation flow conditions are expected to affect the delivery and deposition of pharmaceutical aerosols. Considering aerosol size distributions, MDIs typically produce a consistent aerosol size across a range of inhalation flow rates (7). In contrast, the size distributions of aerosols from DPIs are known to be dependent on inhalation flow rates (4,7), with some inhalers showing more sensitivity than others (8,36). Studies reporting MT deposition of MDI aerosols have shown that deposition decreases with increasing flow rate in the range of 30 to 90 L/min (37,38). For DPIs, Finlay and Gehmlich (39) reported aerosol size was not significantly different when considering transient inhalation waveforms *vs.* square waveforms commonly used for *in vitro* testing with constant time-averaged flow rates for two devices. Considering a device with an intermediate resistance (Novolizer), *in vitro* MT and upper TB deposition were reported to be primarily a function of flow rate, as well as the flow waveform (40,41). From *in vivo* studies, inhalation flow rates and waveforms with current MDI and DPI devices are known to be highly variable (41,42). However, the effect of this variability on the relative performance of MDIs and DPIs in terms of lung delivery and TB deposition is currently not known.

The objective of this study is to compare MDI and DPI aerosol deposition in the entire conducting airway region using a combination of *in vitro* experiments and a newly proposed SIP model for correct and incorrect inhalation flow conditions. Waveforms representing correct and incorrect usage of the MDI and DPI are developed from the literature. Concurrent *in vitro* experiments are used to determine the size distributions of the MDI and DPI aerosols. The numerical model begins at the site of aerosol formation and extends through the 15th bifurcation of each lung lobe, which represents the terminal bronchioles. Validation studies are presented comparing predicted deposition in the MT and upper TB region with concurrent *in vitro* results for an identical geometry. In comparison, the previous study of Tian *et al.* (34) only considered a characteristic DPI with SIP transport into one lung lobe for a single inhalation profile with a focus on the model development aspects of steady state *vs.* transient flow and sampling the airways. The MDI and DPI devices considered in the current study deliver the drug (fluticasone propionate) at an identical nominal dose (250 μg). Considering the correct inhalation waveform for each inhaler, CFD results may indicate which device is more efficient at delivering the drug to the TB airways, i.e., the site of action. Consideration of incorrect waveforms may show which device is most sensitive to this form of patient error. Furthermore, regional deposition predictions by CFD may indicate preferences in the devices for treating asthma manifesting at different levels of the TB airways on a patient-specific basis or for delivering aerosols to different portions of the lungs.

MATERIALS AND METHODS

Inhalers and Airway Model

The Flovent HFA MDI and Flovent Diskus DPI (both GlaxoSmithKline, Raleigh, NC) were selected as commonly prescribed inhalers delivering fluticasone propionate at a dose of 250 μg. The Flovent MDI is a suspension formulation and has a metered dose of 250 μg and an emitted dose of 220 μg, indicating an approximate 12% drug loss in the device. Micronized fluticasone propionate, which is non-hygroscopic, is suspended in HFA 134a with no other excipients and has a total metered mass of 75 mg per actuation. The Diskus DPI delivers 250 μg as a single dose of micronized fluticasone propionate in a powder blend with 12.5 mg of lactose.

Models of the Flovent MDI and DPI connected to characteristic geometries of the MT, upper TB region through the third bifurcation (B3), and lower TB pathways extending to the terminal bronchioles (B15) are displayed in Fig. 1. The numerical model of the MDI includes the actuator with air entering around the canister, mixing with HFA spray from the nozzle, and exiting the actuator mouthpiece. The inner diameter of the spray nozzle was determined to be 0.5 mm, based on measurements. The numerical model of the DPI consists of a 5 mm orifice through which the powder is aerosolized and delivered to the patient, the inhaler mouthpiece, and two small 0.5 mm air jets, which appear to be designed to reduce mouthpiece deposition. Including the flow pathways and mouthpieces for both inhalers was considered important in order to accurately capture deposition within these devices and to generate accurate inlet conditions for the airway model.

The inhalers are connected to a characteristic MT geometry based on the elliptical model originally proposed by Xi and Longest (43). This MT model was developed from the oral airway cast reported by Cheng *et al.* (44) and in-house CT data of the pharynx and larynx. The original inlet diameter of the MT model was 22 mm, which was considered similar to the MDI mouthpiece height of 16 mm.

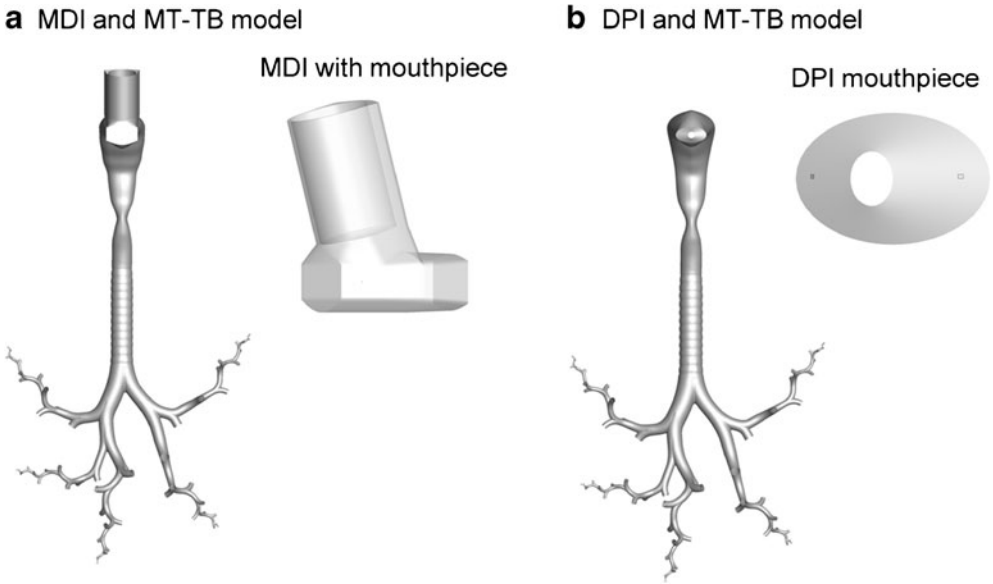

Fig. 1 Surface models of the mouth throat (MT), upper tracheobronchial (TB) airways through the third bifurcation (B3), and stochastic individual paths (SIPs) extending into each of the five lung lobes connected to the Flovent (**a**) metered dose inhaler (MDI) and (**b**) dry powder inhaler (DPI).

As a result, the MT geometry was smoothly connected to the inhaler assuming an insertion depth of 0.5 cm. For the DPI considered in this study, the mouthpiece has a leading edge height of 12 mm. To account for this more closed mouth position, the top and bottom profiles of the oral cavity were both moved inward 5 mm. The inhaler was then connected to this reduced volume oral cavity. The pharyngeal and laryngeal regions of the MT model were not altered. The resulting MT volumes for the MDI and DPI geometries were 57.7 and 55.0 cm^3, respectively.

The upper TB airways are represented with a characteristic model extending through the third bifurcation. This asymmetrical model was based on the anatomical cast dimensions reported by Yeh and Schum (45) and scaled to a functional residual capacity (FRC) of 3.5 L, which is consistent with an adult male (46). The individual bifurcation units were generated using the physiologically realistic bifurcation (PRB) parameters reported by Heistracher and Hofmann (47). However, modifications to the equations reported by Heistracher and Hofmann (47) were required to generate smooth asymmetrical bifurcations. Surface properties of the bifurcations such as carinal ridge and branch radii of curvatures were taken from the measurement studies of Horsfield *et al.* (48) and Hammersley and Olson (49). These bifurcation units were rotated out of plane to approximate the gravity angles specified by Yeh and Schum (45). The upper TB model was extended to the third bifurcation (B3 with the trachea and main bronchi representing B1) to generate a conservative number of branches along each flow path. The resulting upper TB model then includes one bifurcation in each of the five lung lobes, except for the right middle and lower lobes, which contain one branch each. Cartilaginous rings were included in the trachea of the TB model and a D-shaped tracheal cross section was implemented. Dimensions of these geometric features were based on in-house medical scans and the cadaver measurements of Russo *et al.* (50), as described by Tian *et al.* (34).

Beyond the third bifurcation, stochastic individual path (SIP) models were considered extending into each of the five lung lobes. Bifurcations within the SIP models were constructed as PRB units with the airway dimensions reported by Yeh and Schum (45), again scaled to a FRC of 3.5 L. An advantage of the Yeh and Schum (45) data is that average dimensions are provided for each lung lobe. Use of the individual path model based on PRB units allows for the application of a hexahedral mesh, which improves solution accuracy and requires fewer cells to adequately resolve the flow domain (51). Based on available data, the bifurcations in the individual path model section (B4-B15) were symmetric and included a symmetric outflow assumption at each bifurcation level. Continuation of the left or right branch of each bifurcation was considered to be consistent with the flow distribution, resulting in an equal probability for the symmetric outflow assumption. However, if the selection led out of the general region of the initial lung lobe, the other branch was selected. Consecutive branches were rotated at 90^o to approximate physiological conditions (52). Bifurcation 15 was assumed to end with the terminal bronchioles in each lobe, based on existing anatomical data (45). The study of Tian *et al.* (34) indicated that one SIP model could resolve the regional and bifurcation averaged deposition efficiency in a lung lobe to within a relative error of approximately 5% for symmetric bifurcations. As a result, one SIP model was considered sufficient to characterize deposition within each of the five lung lobes.

Inhalation Waveforms

The package inserts for the MDI and DPI instruct the user to inhale "slowly and deeply" and "quickly and deeply", respectively. Characteristic inhalation waveforms to represent slow and deep (SD) and quick and deep (QD) breathing with these inhalers are needed. Parameters describing transient inhalation waveforms are defined in Table I. Inhalation waveforms during inhaler use have recently been recorded and reported by Byron *et al.* (40), Delvadia *et al.* (41), and Olsson *et al.* (53). Common characteristics among the reported waveforms are a nearly linear acceleration to peak flow followed by a sinusoidal pattern during deceleration. Furthermore, the peak inspiratory flow rate (PIFR) typically occurs during the first 1/6 to 1/4 of the inhalation period. Equations describing this waveform pattern are

$$Q(t) = \frac{PIFR}{T_{PIFR}} t \quad 0 \le t \le T_{PIFR} \tag{1}$$

$$Q(t) = PIFR \cos\left(\frac{2\pi(t - T_{PIFR})}{4(1 - TF_{PIFR})T}\right) \quad T_{PIFR} < t \le T \tag{2}$$

$$\overline{Q} = \frac{1}{T}\int_0^T Q(t)dt \tag{3}$$

where all parameters are defined in Table I. To describe the SD and QD waveforms, 3 parameters are required. The remaining parameters are then derived from the waveform shape. In this study, deep inhalation is represented by a 3 L inhaled volume. This value is consistent with the study of Broeders *et al.* (42), who report an approximate 3 L inhalation volume with the use of both a DPI (Diskus) and MDI for stable asthmatic and mild to moderate COPD patients. The mean inhalation flow rate was also a defined parameter to allow for comparisons between steady state and transient deposition results. A mean inhalation flow rate of 75 L/min was selected for the QD profile, as a typical value for DPI steady state testing. A mean inhalation flow rate of 37 L/min (which is approximately one half the QD value) was selected to represent SD inspiration. Based on observations from reported waveforms as described above, the time fractions to peak inspiratory flow rate (TF_{PIFR}) for the SD and QD waveforms were 1/4 and 1/6, respectively. Equations to find the remaining inhalation parameters are shown below.

$$V[L] = \frac{PIFR[L/\min] \times T_{PIFR}}{2 \times 60} + \int_{T_{PIFR}}^{T} \frac{PIFR}{60} \cos\left(\frac{2\pi(t - T_{PIFR})}{4(1 - TF_{PIFR})T}\right) dt \tag{4}$$

$$T[s] = \frac{60V[L]}{\overline{Q}[L/\min]} \tag{5}$$

Results from solving these equations for the SD and QD parameters are reported in Table II. The resulting PIFRs for the QD and SD profiles are 122.2 L/min and 61.4 L/min, respectively. For the Diskus DPI, Broeders *et al.* (42) observed a characteristic PIFR of approximately 120 L/min after training among 42 patients with stable asthma and mild to moderate COPD. Van der Palen (54) observed an average PIFR of 118 L/min for Diskus among 50 patients that received medication for asthma and COPD. Byron *et al.* (2010) reported a PIFR of approximately 120 L/min for a single healthy subject with a Novolizer DPI, which has a similar resistance compared with the Diskus. As a result, the PIFR of the Diskus appears consistent with literature data for both healthy and asthmatic/COPD patients. Considering the MDI, the typical recommended PIFR for correct usage is between 25 and 90 L/min (42). Furthermore, Ross and Schultz (7) showed that inhalation flow rate had little effect on MDI drug delivery. The PIFR of the MDI (i.e., 61.4 L/min) is approximately in the middle of the recommended range and therefore a representative approximation of correct usage. As a result of this analysis, correct inhaler usage is considered to be the SD profile with the MDI and the QD

Table I Parameters Describing Transient Inhalation Waveforms

Parameter	Units	Description
PIFR	L/min	Peak inhalation flow rate
Q(t)	L/min	Transient inhalation flow rate
$\overline{Q}$	L/min	Mean inhalation flow rate
T	s	Period of inhalation
T_{PIFR}	s	Time to peak inhalation flow rate
TF_{PIFR}	–	Time fraction of peak inhalation flow rate
V	L	Total volume inhaled

Table II Waveform Parameters for the QD and SD Profiles

Parameters	QD Profile	SD Profile
PIFR [L/min]	122.2	61.4
$\overline{Q}$ [L/min]	75	37
T [s]	2.40	4.86
T_{PIFR} [s]	0.40	1.22
TF_{PIFR}	1/6	1/4
V [L]	3	3

profile with the DPI. In contrast, incorrect inhaler use is often associated with inhaling too quickly through an MDI and too slowly through a DPI. As a result, incorrect inhaler use will be assessed using the QD profile for the MDI and the SD profile with the DPI in this study.

Experimental Procedure

In vitro experiments were conducted to evaluate the aerosol size distributions leaving the inhalers and to calculate deposition in the inhaler, MT and upper TB airways through B3. For the size distribution experiments, the inhalers were actuated into a preseparator connected to a Next Generation Impactor (NGI; MSP Corp., Shoreview, MN) with flow generated using a vacuum pump. The mouthpieces of both inhalers were connected to the preseparator using an adapter to ensure an airtight seal. Considering the MDI aerosol, the inlet flow rate is not expected to significantly affect the size distribution for typical inhalation values (7). As a result, a steady inhalation flow rate of 30 L/min was used with continuous air flow. In contrast, inhalation flow rate is known to influence the size distribution of many DPI aerosols. Square wave inhalations of 37 and 75 L/min for 4 s were generated using a 3-way solenoid valve connected downstream of the NGI. For both the MDI and DPI experiments, impactor stages and the preseparator were coated with silicone to prevent particle bounce and re-entrainment. Drug deposition in the impactor was determined using the USP HPLC assay method for fluticasone propionate for five single dose experiments with both the MDI and DPI. Particle size distributions were reported as fluticasone propionate mass distribution recovered in the impactor. The mass median aerodynamic diameter (MMAD) was defined as the particle size at the 50th percentile on a cumulative percent mass undersize distribution (D50) using linear interpolation.

For CFD model validations, an exact replica of the MT-TB model used in the CFD simulations through the third bifurcation (B3) was constructed using in-house rapid prototyping facilities (Viper SLA Machine; 3D Systems, Valencia, CA). The model was constructed with clear Accura 60 plastic resin using a build layer thickness of 0.15 mm and a laser spot diameter of 0.25 mm. Figure 2 illustrates the MDI and DPI connected to the MT portion of the airway model. The inhaler and the MT were connected to the upper TB model through B3, which was housed in a custom-built plexiglass chamber with minimal dead space and connected to a three-way solenoid valve and vacuum pump as previously described by Byron *et al.* (40). For each test, the inhaler was primed to waste, cleaned and then inserted into the mouth opening. An airtight seal between the inhaler mouthpiece and the MT-TB model was maintained. The internal surfaces of the MT-TB model were coated with a glycerol:methanol (1:2 by volume) mixture, followed by methanol evaporation

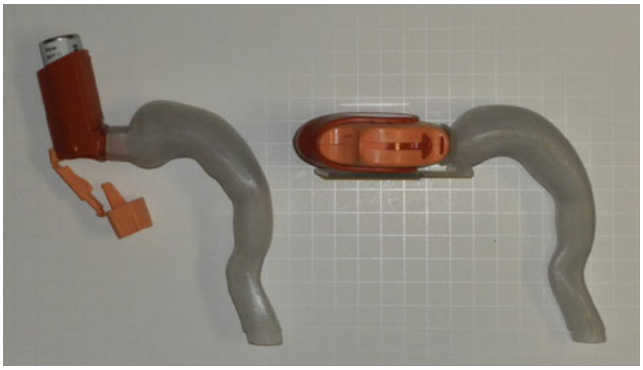

Fig. 2 Flovent HFA 134a MDI and Flovent Diskus DPI inserted into the characteristic MT geometry used for *in vitro* testing of aerosol deposition.

before each experiment. A low resistance filter was placed in-line to retain aerosolized drug that passed through the model and exited the plexiglass chamber. The inhalation profile for the MDI experiments was a steady state flow rate of 37 L/min, which represents the time-averaged value of the SD waveform. For the DPI, a square wave inhalation profile of 75 L/min for 4 s was implemented to represent the time-average of the QD profile. Drug masses retained in the MT, TB, and plexiglass housing plus filter were calculated following recovery using a wash solution and analysis for fluticasone propionate by the USP HPLC assay method.

CFD Simulations

Boundary conditions implemented for both inhaler systems include constant wall temperatures and pre-determined outlet flow distributions. Outflow boundary conditions from the upper TB model were based on estimates of ventilation to each lung lobe. Lobar ventilation approximations presented in the studies of Horsfield *et al.* (55), Asgharian and Price (56), and Yin *et al.* (57) were considered. Reasonable consistency among these studies led to the following distribution estimates for each of the five lung lobes: right upper 14%, right middle 7%, right lower 33%, left upper 15%, and left lower 31%. The resulting right and left ventilation proportions were 54 and 46%, respectively. Beyond the lobar bronchi, symmetric outflow conditions were assumed at each bifurcation level (B4-B15). This assumption is not expected to largely influence the regional and local deposition characteristics of interest in this study.

For the MDI, inlet air and formulation flows were prescribed as mass flow rates over time. Based on literature values, the expected spray time of the MDI was 0.2 s (58). The actuation timing for the MDI was assumed to be centered on the mean accelerating flow ($T_{a\text{-}mean}$ in Fig. 3) resulting in firing times of 0.63–0.83 s for the SD waveform and 0.15–0.35 s for the QD waveform. To estimate initial

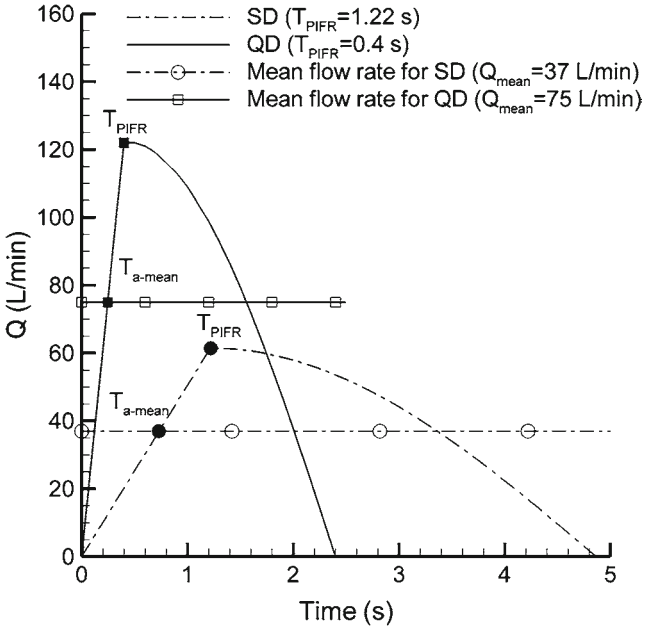

Fig. 3 Characteristic inhalation waveforms for slow and deep (SD) and quick and deep (QD) breathing with inhalers. Based on package insert instructions, the SD and QD profiles are considered to be the correct inhalation techniques for the MDI and DPI, respectively.

conditions of the spray, isentropic flow through the nozzle was considered. The formulation exiting the nozzle was assumed to be at the HFA 134a boiling point for atmospheric pressure and traveling at sonic velocity (i.e., choked flow conditions). Conservation of mass was used to estimate an approximate density of the slurry exiting the nozzle. The thermodynamic pressure at the nozzle exit was determined from the ideal gas law and found to be 123.0 kPa based on HFA 134a properties. This very high static pressure at the nozzle exit experiences a sudden expansion as it adjusts to atmospheric conditions, which can further accelerate the flow, create significant droplet inertia and breakup, and induce significant shear stresses in the flow field.

Considering the DPI, a blunt velocity profile was assumed at the 5 mm aerosol jet orifice and constant velocity inlets were assumed at the 2 smaller jet inlets. Pressure *vs.* flow experiments indicated that approximately 10% of the air entered through the small jets. Experiments also indicated that the powder emptied from the inhaler during the first 0.5 s of airflow with a square wave at 75 L/min. However, the bulk of the DPI powder likely empties around the mean accelerating flow with the SD and QD waveforms. As a result, a 0.5 s emptying period was assumed to be centered on the time of mean accelerating flow resulting in a release of particle for the QD profile between 0 and 0.5 s and for the SD profile between 0.48 and 0.98 s. Release of the particles for the SD waveform between 0 and 0.5 s was also considered for the DPI.

Flow fields in both inhaler systems include high speed turbulent jets, transient flow, and multiple phases. The MDI includes the added complexities of compressible supersonic flow near the nozzle, heat transfer, multiple species (air and HFA 134a), and large changes in scale between the nozzle tip (0.5 mm) and MT inlet (~1.6 cm). To address these complex flow conditions and calculate a solution over the entire breathing cycle (~ 3 s), a low Reynolds number (LRN) k-ω turbulence model was selected. This model has previously been well tested, and found to provide good estimates of aerosol transport and deposition in upper airway geometries (59,60). To evaluate the variable temperature and specific concentration fields in the MT-TB model, interconnected relations governing the transport of heat and mass (HFA 134a) were also included. These governing equations were previously presented in detail by Longest and Xi (22) and Longest *et al.* (61). In addition to the monodisperse particle deposition studies indicated above, the LRN k-ω approach has also been shown to provide good estimates of transport and depostion for pharamacutical aerosols generated with a DPI (34) and spray devices including a MDI and softmist inhalers (61–63).

A Lagrangian particle tracking model was employed to determine the trajectories of individual particles, turbulent dispersion, and deposition. This model was implemented using a previously developed combination of a commerical code (Fluent 12, ANSYS, Inc.) and user functions. User routines were employed to better model near-wall conditions and to simulate aerosol deposition in the complex three-dimensional multi-scale flow field. Previous studies have shown that the isotropic turbulence approximation, which is assumed with the LRN k-ω model, can over predict aerosol deposition (64). As a result, a user routine was employed to account for anisotropic near-wall turbulence, as previously described by Longest *et al.* (61). Other additions to the particle tracking model included (i) a correction to better predict the Brownian motion of submicrometer aerosols and (ii) improved near-wall interpolation of fluid velocities (65).

Considering heat and mass exchange between the particles and air, the DPI aerosol was considered stable due to the non-hygroscopic nature of fluticasone propionate. In contrast, MDI droplets composed of liquid HFA 134a and suspended drug particles are known to rapidly evaporate (66). Knowledge of the droplet size distribution near the spray nozzle is very difficult to obtain due to rapid change and small time scales. It is expected that the aerosol size distribution measured at the NGI is for dry particles containing only fluticasone propionate. As a method to predict MDI deposition without accurate knowledge of the initial droplet diameters, the final dried size distribution was assumed to exit the MDI nozzle in the CFD simulations. The particles were then modeled without considering size change.

The adequacy of this assumption will be assessed by comparing the numerical predictions with the experimental deposition results.

The timing of particle release is expected to affect aerosol deposition (67). Experiments indicated that the DPI emptied in approximately 0.5 s with the application of a square wave profile and the MDI has a firing time of 0.2 s. As a first approximation, the CFD model implements these release times and assumes that they are centered on the mean accelerating flow for the two waveforms considered ($T_{a\text{-}mean}$ in Fig. 3). The effects of this assumption are evaluated by considering a second release condition in which the aerosol is initially introduced at t=0 and injected continually until 0.2 and 0.5 s for the MDI and DPI, respectively. Based on the findings of Tian *et al.* (34), a constant rate of aerosol release is considered in all cases.

In performing the CFD simulations, previously established best-practices were implemented to provide a high quality solution. All transport equations were discretized to be at least second order accurate. The computational mesh was constructed in Gambit 2.4 (ANSYS, Inc.) and consisted entirely of hexahedral elements, which provide a higher quality solution than commonly employed tetrahedral grids (51,68). Grid convergence based on maximum velocity and deposited drug mass was established for approximately 1.4 million and 1.8 million control volumes in the upper TB model extending to B3 for the DPI and MDI, respectively. Grid convergence was also established for approximately 650 k elements in each individual SIP model. As a result, the total MDI and DPI meshes contained 5.1 and 4.7 million elements, respectively. In order to produce convergent deposition results with the MDI through B3, 72,000 and 90,000 particles for the steady state and transient models were released at the spray nozzle with a uniform distribution. For the DPI, steady and transient simulations implemented 36,000 and 90,000 particles, respectively, for simulations in the MT through B3.

To improve numerical efficiency and accuracy, each SIP geometry was divided into segments B4-B7 and B8-B15. Flow fields were interpolated between the upstream outlets and the inlets of each of these sections. Numerical testing indicated that deposition in the SIP models was nearly identical between the injection of interpolated particle profiles at each SIP inlet and profiles consistent with the inlet velocity field. As a result, particle profiles consistent with the inlet velocity field were implemented, which allowed for the inclusion of additional particles to ensure converged results. Based on this finding, 450,000 particles were injected at the inlet of each SIP section with a concentration profile consistent with the inlet velocity field. Monodisperse particles were used in the SIP geometries with inlet sizes equal to the mass median aerodynamic diameter (MMAD) of each upper TB model outlet. Polydisperse aerosol distributions were implemented in the MT and upper TB airways through B3.

Deposition Predictions

Deposition within regions of the respiratory tract can be reported as either a fraction or efficiency. The deposition fraction (DF) for the i-th region based on drug mass is calculated as

$$DF_i = \frac{mass\ of\ drug\ depositing\ in\ region\ i}{mass\ of\ drug\ entering\ the\ mouth} \tag{6}$$

The corresponding deposition efficiency (DE) for region i is calculated as

$$DE_i = \frac{mass\ of\ drug\ depositing\ in\ region\ i}{mass\ of\ drug\ entering\ region\ i} \tag{7}$$

To determine a total deposition fraction, DF_i values in individual regions can be directly summed. Deposition efficiency values are an effective method to report the characteristics of an individual section of the respiratory tract without the influence of upstream aerosol losses. In this study, DE values are calculated for each bifurcation based on deposited drug mass. Sectional DE values are then computed by combining the individual bifurcation values (46). For example, the DE in region B4 to B15 within a single lung lobe is calculated as

$$DE_{B4-B15} = 1 - (1 - DE_{B4})(1 - DE_{B5})... \\ (1 - DE_{B14})(1 - DE_{B15}) \tag{8}$$

The deposition fraction within an individual lung lobe is then calculated as

$$DF_{lobe} = DE_{lobe} * FR_{lobe} \tag{9}$$

Where FR_i represents the fraction of aerosol remaining at the inlet of the i region (i.e., lung lobe). The total deposition fraction within the MT-TB model is then the sum of the DF values in the MT, upper TB region, and within each of the five lung lobes.

Based on the results of Tian *et al.* (34), transient simulations are required in the upper airways through approximately B3, whereas steady state approximations are acceptable in the SIP models. In this study, transient SD and QD simulations are conducted for the inhalers, MT and upper TB airways using the SD and QD waveforms. For the individual SIP models, steady state simulations are then performed at the equivalent mean flow rates. In these steady state simulations, the inhalers and upper MT-TB models are included to generate approximate flow fields and particle conditions at the inlet to each of the SIP geometries.

Deposition efficiencies determined with the transient simulations for the MT-TB model are then combined with the SIP values using the equations described above to characterize deposition throughout the conducting airways. Tian *et al.* (34) showed that this approach was accurate to within 5% of fully transient simulations in both the upper and lower airways, but provided a significant savings in solution time.

RESULTS

Aerosol Size Distributions and Validations

Aerosol size distributions for the MDI and DPI are reported in Fig. 4 as a function of midpoint diameters for the stages of the NGI and the preseparator cutoff diameter. Based on the absence of a large particle mode on the upper stages for the MDI, the measured distribution likely indicates a fully dried aerosol (69). At the sampling flow rate of 30 L/min, the MDI aerosol had a mass median aerodynamic diameter (MMAD) of 2.64 μm with a standard deviation (SD) of 0.1 and a geometric standard deviation (GSD) of 1.51. The drug mass distribution from the DPI consisted of approximately 70% from particles greater than 10 μm and 30% from smaller particles. The smaller size fraction represents deaggregated drug particles that have separated from the larger lactose carrier, whereas the larger fraction represents drug particles still attached to lactose and drug particle agglomerates. With a flow rate of 75 L/min, the MMAD (SD) of the DPI aerosol based on drug mass was 2.99 μm (0.2) with a GSD of 2.09. Reducing the flow rate to 37 L/min resulted in less separation among the particles and a larger MMAD (SD) of 4.10 μm (0.05) with a GSD of 2.13. The exact size range of the particles depositing in the preseparator is not known as there is no upper size limit. As an approximation, the CFD model implemented the preseparator cutoff diameter as the largest size bin of particles considered. This assumption is not expected to have a significant impact on the results as these upper sizes and the constant proportion of drug mass associated with them are typically deposited in the MT region.

Computational fluid dynamics (CFD) predictions of deposited drug mass are compared with *in vitro* results for the MDI in Fig. 5 under steady flow conditions. Good agreement between the predicted results (CFD) and experimental (exp) data is observed within the three regions representing the inhaler actuator, MT, and upper TB geometry. As a result, the CFD model appears to accurately predict the deposition of drug mass from the polydisperse aerosol in this highly complex system. Furthermore, this comparison indicates that the assumptions of fully dry particles at initialization and conditions at the spray nozzle outlet are adequate for predicting the deposition of drug mass for the MDI.

Tian *et al.* (34) previously reported a comparison of CFD model predictions and experimental results for the Diskus DPI. Predicted *vs.* experimental values showed good agreement in the MT (DF_{CFD}=65.2% *vs.* DF_{exp}=72.5%) and upper TB (DF_{CFD}=2.3% *vs.* DF_{exp}=2.2%) regions. It was found that adequate predictions required the simulation of the square transient input waveform implemented in the DPI experiments. This comparison provides confidence that the particle distribution is adequately characterized by the model and that the flow field is well resolved over a transient input waveform.

Characterization of Flow Fields

Velocity vectors and contours of velocity magnitude at the midplane of the MT and upper TB region are reported in Fig. 6 at mean accelerating flow. The top two panels

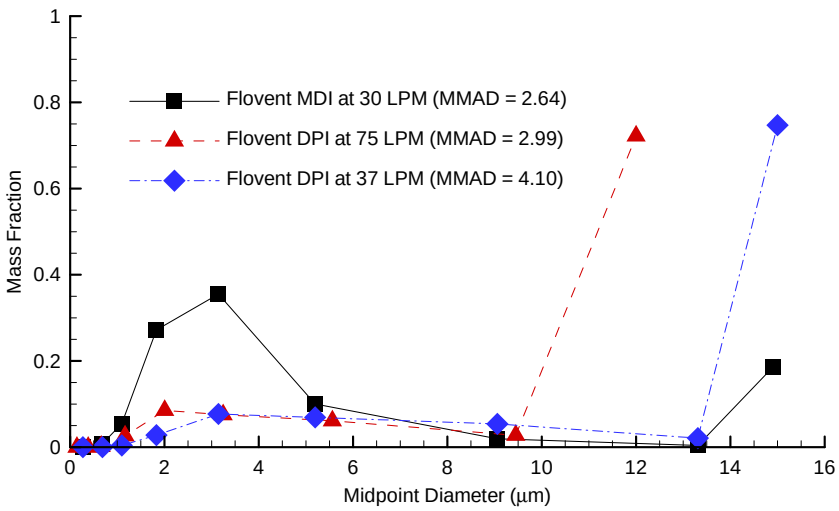

Fig. 4 Mass fraction distribution for the Flovent MDI (measured at 30 L/min) and DPI (measured at 37 and 75 L/min) based on emitted dose from the inhaler.

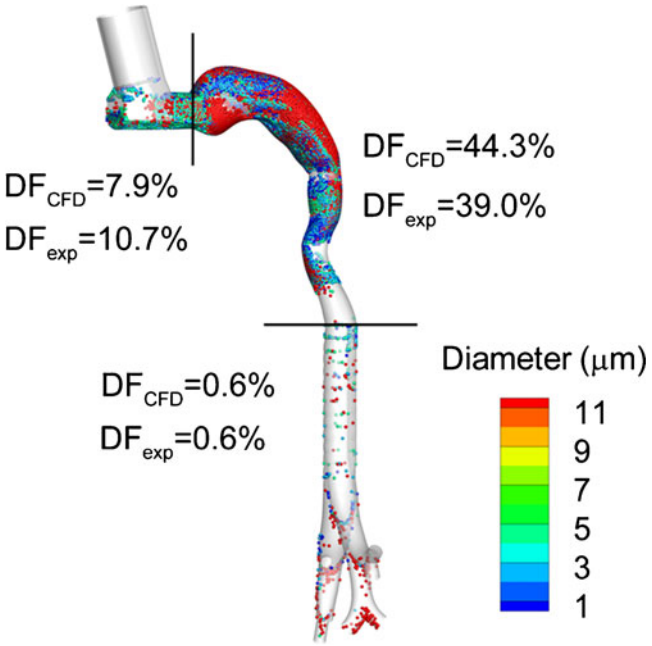

Fig. 5 Comparison of deposited drug mass from the *in vitro* experiments and CFD predictions for the MDI. Good agreement between the model predictions and experimental results is observed in the inhaler, MT and upper TB regions.

(Fig. 6a and b) compare the MDI and DPI flow fields for correct inhalation profiles of SD and QD, respectively. Compared with the large recirculation zone created by the DPI in the MT region, a much smaller region of recirculating flow is observed for the MDI due to lower velocities and a larger air inlet. Considering incorrect inhalation profiles (Fig. 6c and d), the recirculation region observed with the MDI remains small. For the DPI with SD inhalation, the velocity magnitude of the turbulent jet is significantly reduced; however, the recirculation region still occludes a large portion of the MT geometry.

Upper Airway Deposition

CFD predictions of MDI and DPI aerosol deposition in the MT and upper TB airways are illustrated in Fig. 7. The upper panels (a and b) represent drug mass deposition with correct inhalation profiles for the MDI and DPI whereas the lower panels (c and d) report deposition with incorrect usage. Considering correct inhalation profiles, the MDI produces approximately one half the MT depositional loss that is observed with the DPI. Considering upper TB deposition, which may be beneficial for upper airway respiratory conditions, the MDI is observed to deliver approximately twice the dose of the DPI through B3. For incorrect inhalation, the MT deposition with the MDI increases by a percent difference of approximately 20% and the TB deposition decreases by 50% compared to correct usage. For the DPI and incorrect inhalation, the MT deposition is unchanged and the upper TB deposition fraction decreases by a percent difference of approximately 40%. Even with incorrect inhalation profiles, the MDI is observed to lose less drug in the MT and deliver more drug to the airways than the DPI with either inhalation profile.

As described, release of the aerosol in the CFD model was assumed to be centered in time on the mean accelerating flow (i.e., mean flow release). However, the effect of aerosol release (or inhaler activation) timing on deposition is also of interest. Additional simulations were conducted in which aerosol release occurred continuously during the first 0.2 and 0.5 s of inhalation for the MDI and DPI, respectively. It is noted that with the DPI and QD inhalation, mean flow release result in a starting release time of 0 s. Compared with mean flow release, starting particles at time zero reduced MT and upper TB deposition by only a small amount (<3% in the MT and <0.4% in the upper TB region). These differences did not affect the relative comparisons of MDI *vs.* DPI deposition under correct and incorrect inhaler conditions that were made for mean flow release. As a result, release time does not appear to affect deposition patterns in the MT and upper TB airways as significantly as inhaler type and inhalation waveform conditions.

Lower Tracheobronchial and Total Deposition

Deposition in the TB airways through B15 for each of the five lung lobes is presented in Figs. 8 and 9. As before, upper panels represent the correct inhalation waveform used with the MDI and DPI. Figure 8 reports deposition efficiencies (DE) and fractions remaining (FR) for the five lung lobes denoted as left upper (LU), left lower (LL), right upper (RU), right middle (RM) and right lower (RL). It is noted that the fraction remaining is reported for the inlet of each lung lobe such that the DF can be calculated as described with Eq. 9. For correct inhalation profiles, the DPI is observed to have approximately 25–50% higher deposition efficiencies in each lung lobe, due to the higher flow rate, compared with the MDI (Fig. 8a *vs.* b). However, FR values with the DPI are approximately one half those observed for the MDI. Considering incorrect inhalation profiles, the relative values of DE are more similar between the MDI and DPI. However, FR values are not largely changed with incorrect inhalation due to small changes in MT deposition. The resulting DFs in each lung lobe are presented in Fig. 9. Considering correct inhalation profiles, the MDI appears to provide higher drug delivery to the B1-B3 region and each of the lobes (Fig. 9a *vs.* b). With incorrect usage, the MDI again provides higher drug delivery to B1-B3 and also provides increased delivery to the individual lung lobes compared with the DPI (Fig. 9c *vs.* d). For all cases considered, the right upper lobe receives the lowest dose

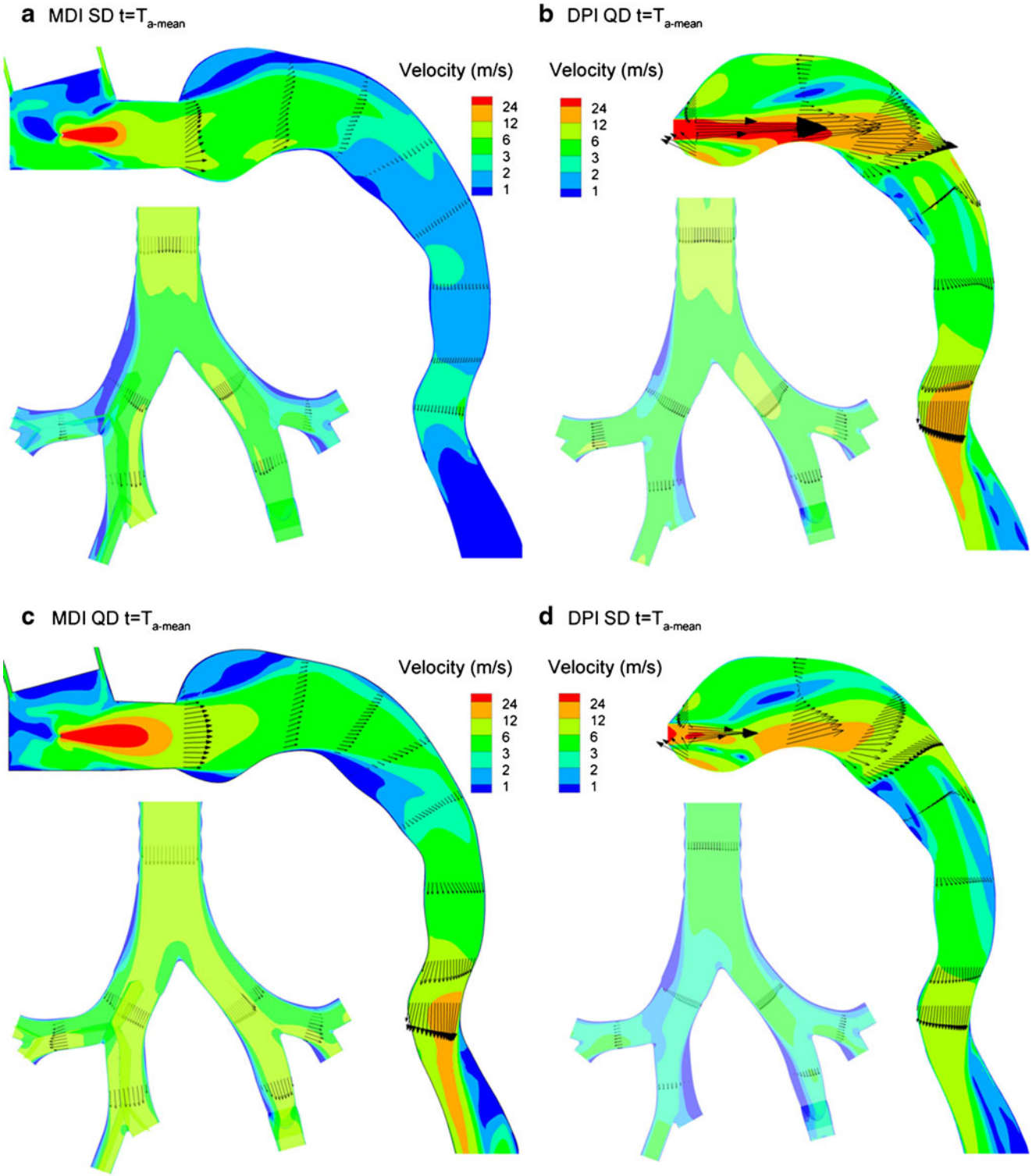

Fig. 6 Contours of velocity magnitude and representative velocity vectors in the midplane of the MT and upper TB geometries with correct inhalation profiles for the (**a**) MDI and (**b**) DPI and incorrect inhalation profiles for the (**c**) MDI and (**d**) DPI. Results in (**b**) were previously reported by Tian *et al*. (34) and are included here for comparison with three other device and inhalation combinations.

of aerosol. The relative dose fraction to the other lobes was variable and dependent on both inhaler type and inhalation profiles.

Deposition fractions as a function of airway region are presented in Fig. 10 on a log scale in order to visualize values across three orders of magnitude. For the correct

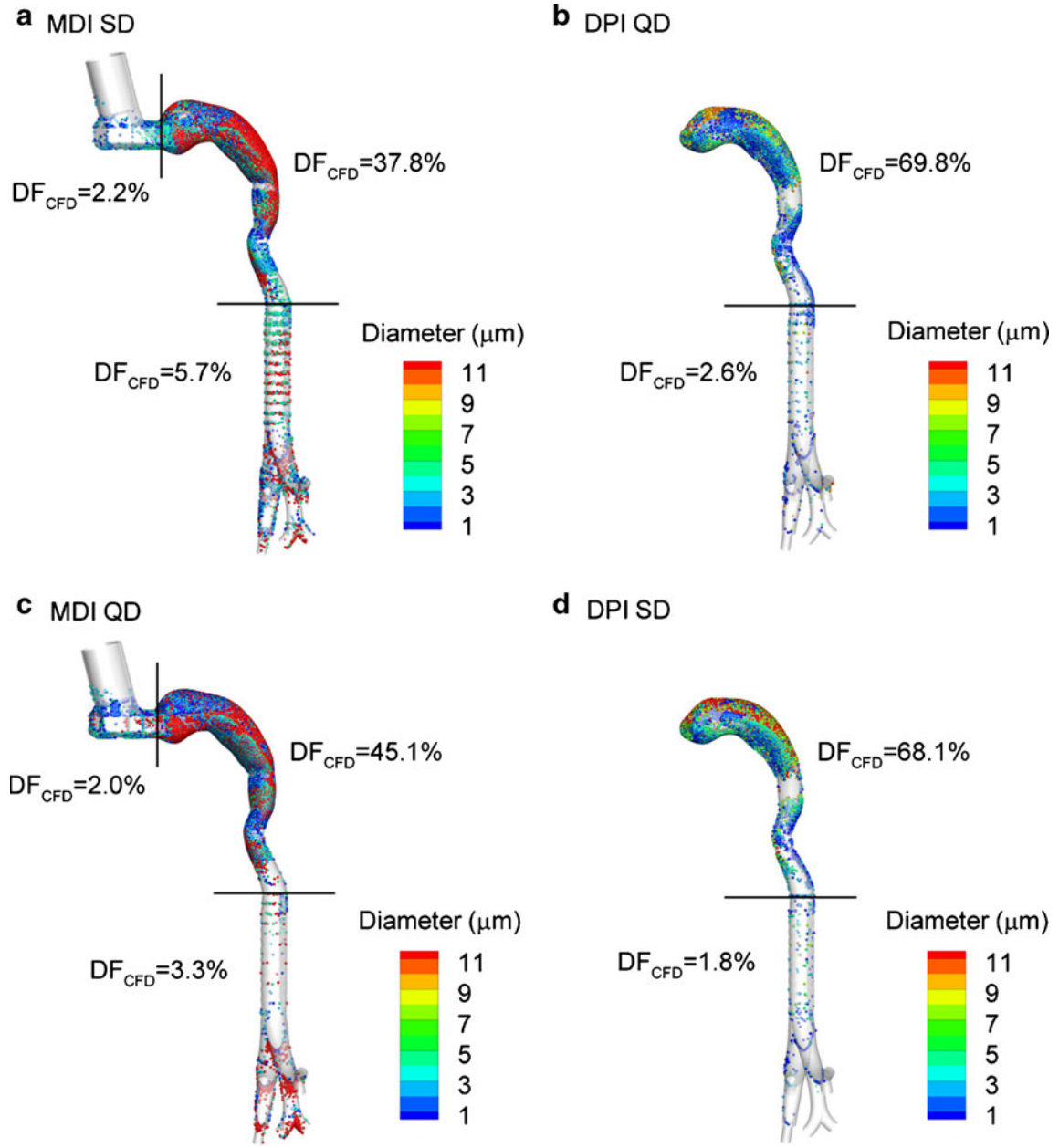

Fig. 7 Deposition fractions (DFs) of drug mass in the MT and upper TB airways predicted for correct inhalations with the (**a**) MDI and (**b**) DPI and for incorrect inhalations with the (**c**) MDI and (**d**) DPI. Results in (**b**) were previously reported by Tian *et al*. (34) and are included here for comparison with three other device and inhalation combinations.

inhalation profiles, the MDI delivers approximately twice the drug dose to each individual TB region compared with the DPI, resulting in approximately 2 times higher total TB dose. Deposition fraction values reported in Table III indicate that for correct usage, the MDI delivers approximately 8.1% of the initial drug to the TB region whereas the DPI delivers approximately 4.2%. For incorrect inhalation, the MDI is again observed to deliver twice the dose to most TB sections and the entire TB region compared with the DPI. From Table IV for incorrect inhalation, the TB deposition fraction for the MDI is 5.8% *vs.* 3.3% for the DPI. Considering the effect of inhalation profile on the delivery from each device, incorrect inhalation reduces the TB dose from the MDI by a 33% difference and decreases the TB dose from the DPI by 24%. These inhalation profile-based differences appear small compared with the factor of 2 difference in TB dose observed between the devices. As a result, it appears that the MDI delivers 2 times more dose the TB region compared with the DPI with a similar reduction in TB dose associated with incorrect usage of both devices.

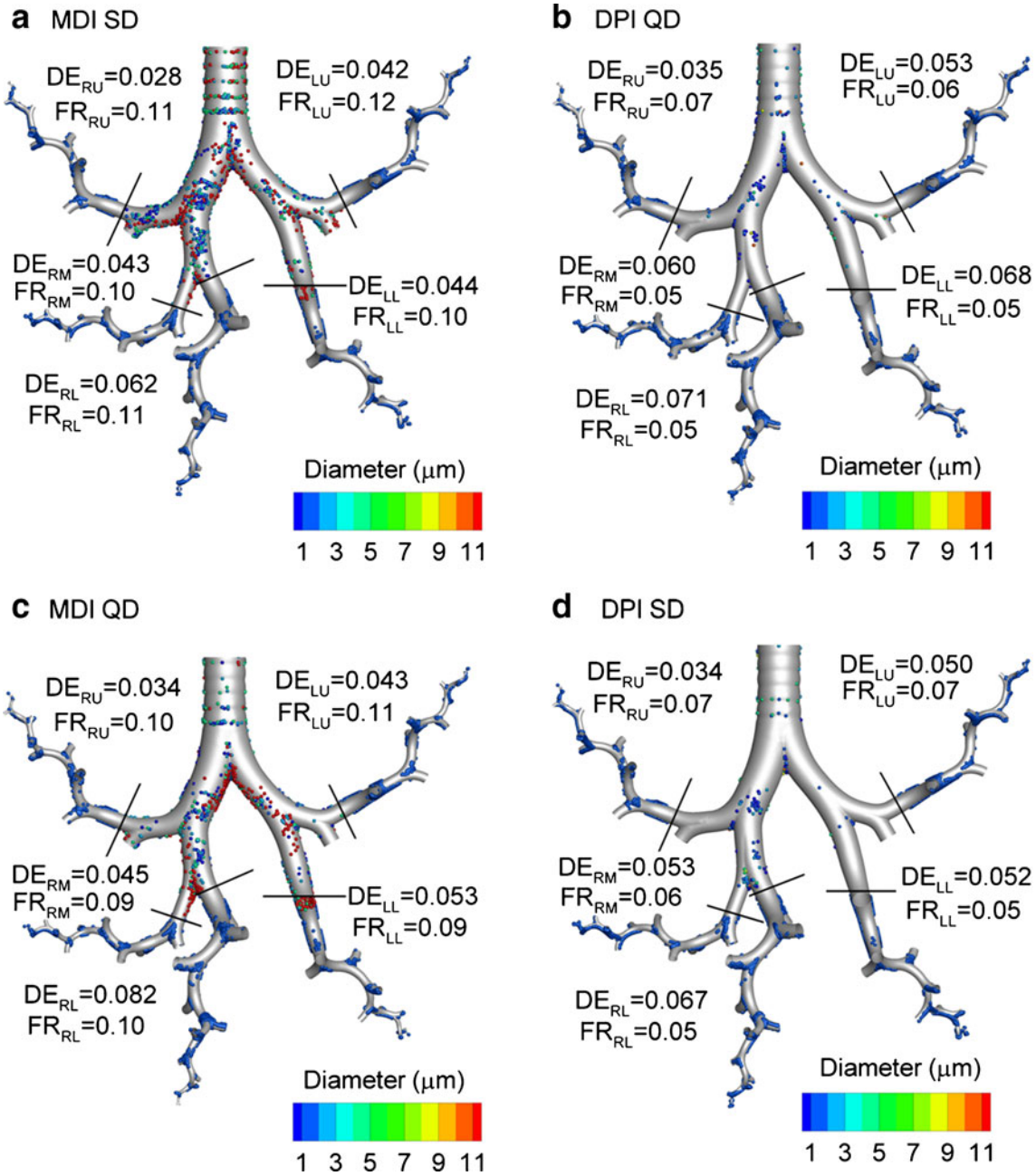

Fig. 8 Deposition efficiencies (DE) within each lung lobe and fractions remaining (FR) at the inlet to each lung lobe for correct inhalation profiles with the (**a**) MDI and (**b**) DPI and incorrect inhalation profiles with the (**c**) MDI and (**d**) DPI.

The inhalation profile employed with each device may potentially be used to modify the deposition within different regions of the airways. The QD profile with the MDI is observed to marginally increase deposition in the region of B4-B7 compared with SD inhalation, while maintaining or reducing delivery to other lung regions. SD inhalation with the DPI is observed to marginally increase deposition in B8-B15 *vs.* the correct QD profile with reductions in all other lung regions. Still, the MDI delivers a higher drug dose to all individual TB regions and the entire TB region for both correct and incorrect profiles. Mouth-throat deposition for the MDI is also two times lower under both inhalation profiles. As a result, it appears that significantly altering regional deposition by modifying the inhalation profile is not practical with a single device and differences obtained are smaller than inter-device differences.

Penetration fractions (PF) are defined as the fraction of the original aerosol dose exiting a specific region, and are reported in Tables III and IV for correct and incorrect inhaler usage. For correct inhalation, the PF values at the

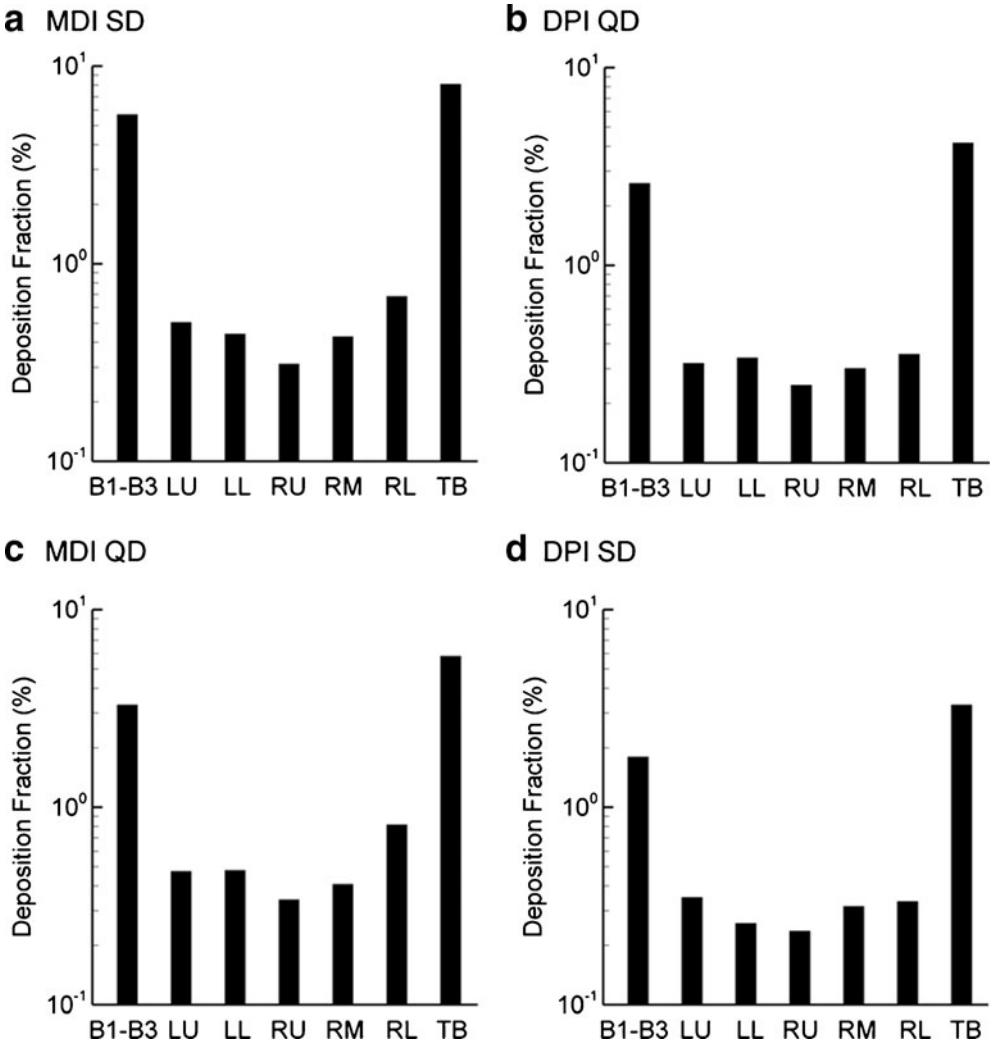

Fig. 9 Deposition fractions (DF as a%) in the upper TB airway and within individual lung lobes for correct inhalation profiles with the (**a**) MDI and (**b**) DPI and incorrect inhalation profiles with the (**c**) MDI and (**d**) DPI.

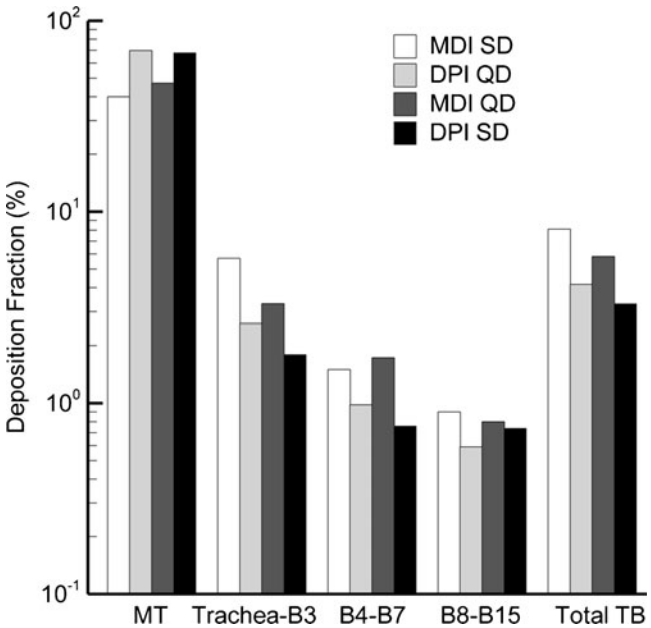

Fig. 10 Deposition fractions (DF as a %) for individual regions of the conducting airways and total TB deposition.

exit of the TB region indicate that the MDI delivers approximately 52% of the initial dose to the alveolar airways whereas the DPI delivers 26.1%. These values are little changed with incorrect inhalation as indicated in Table IV (MDI: 47.1% and DPI: 28.6%). As a result, the MDI delivers approximately 2 times more dose compared with the DPI and nearly 50% of the inhaled aerosol to the alveolar airways regardless of inhalation profile.

Figure 11 illustrates the deposition of drug in bifurcations B4-B15 for each of the inhalers and inhalation profiles that were considered. With the SIP geometries starting at B4, the MDI with QD inhalation is observed to have higher deposition fractions through approximately B7 compared with the correct SD inhalation. Starting with B7, SD inhalation with the MDI produces higher DFs than QD inhalation. The DPI displays a similar trend with higher DFs through approximately B7 using QD inhalation and higher DFs in B8-B15 using SD inhalation. These flow rate dependent differences are largest in the higher bifurcations due to increased inertial deposition and decrease as sedimentation

Table III Deposition Fractions (DF) and Penetration Fractions (PF) at the Outlet of Individual Airway Regions with Correct Inhalation (MDI with SD and DPI with QD)

Region	DF		PF	
	MDI	DPI	MDI	DPI
MT[a]	0.4	0.698	0.6	0.302
Trachea-B3	0.057	0.026	0.543	0.276
B4-B7	0.015	0.010	0.528	0.267
B8-B15	0.009	0.006	0.519	0.261
Total TB	0.081	0.042	0.519	0.261

[a] Includes deposition from the MDI inhaler

becomes the predominant deposition mechanism in the lower bifurcations. On a branch-averaged basis, MDI deposition fractions are higher in all cases except for a small region at B12 to B13.

As with the upper airways, the effect of aerosol release time on deposition in the lower TB airways was also considered. Again, mean flow release was compared with aerosol release beginning at the start of inhalation. Compared with mean flow release, initial release at $t=0$ results in small changes in lobar DFs with differences less than 0.2% for the MDI and <0.1% for the DPI. Regional differences in DFs between the two release conditions were also small. As a result, the timing of aerosol release does not appear to affect the relative differences observed regarding MDI *vs.* DPI aerosol deposition for correct and incorrect inhalation profiles.

DISCUSSION

This study is the first to implement a CFD approach to evaluate the transport dynamics and deposition profiles for two commonly used inhalers under different breathing conditions from the site of aerosol formation through the entire

Table IV Deposition Fractions (DF) and Penetration Fractions (PF) at the Outlet of Individual Airway Regions With Incorrect Inhalation (MDI with QD and DPI with SD)

Region	DF		PF	
	MDI	DPI	MDI	DPI
MT[a]	0.471	0.681	0.529	0.319
Trachea-B3	0.033	0.018	0.496	0.301
B4-B7	0.017	0.008	0.479	0.293
B8-B15	0.008	0.007	0.471	0.286
Total TB	0.058	0.033	0.471	0.286

[a] Includes deposition from the MDI inhaler

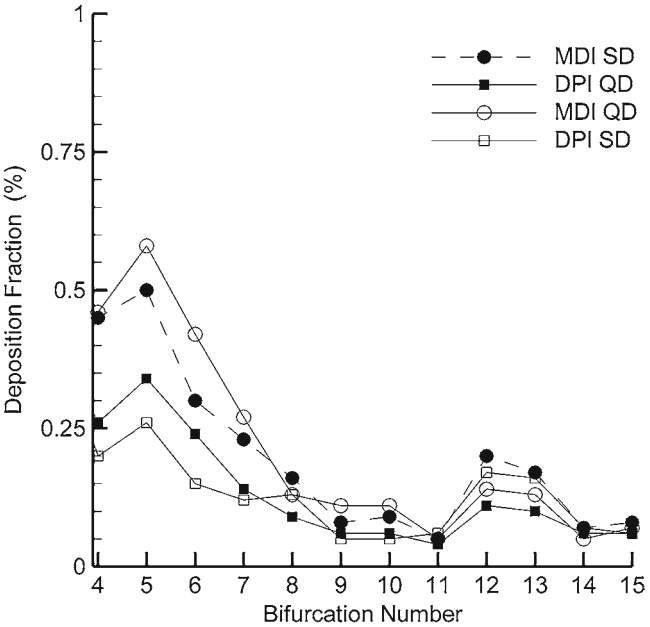

Fig. 11 Deposition fractions (DF as a %) within individual bifurcations evaluated for all five lung lobes from B4 through the terminal bronchioles (B15).

tracheobronchial airways. Due to the complexity of the aerosol formation process, *in vitro* experiments were used to specify the initial particle profiles at the spray nozzle inlet of the MDI and DPI jet. This study is also the first to validate simulations of an MDI aerosol with *in vitro* results in a characteristic model of the MT-TB airways. Large differences in the delivery characteristics of the two inhalers were observed in terms of MT deposition and alveolar delivery. In the TB region, the MDI consistently delivered 2 times more dose than the DPI with both devices showing very similar reductions in dose associated with incorrect inhalation (~30%). These results illustrate advantages of the developed CFD model in terms of predicting regional, branch-averaged, and highly localized deposition of drug from multiple platforms under different inhalation profiles. Furthermore, deposited particle size distributions are predicted on a localized basis, which can be used as a starting point for simulating dissolution, spreading, and absorption of the drug.

The CFD model developed in this study may play a valuable role in the areas of inhaler design, selecting appropriate inhalation devices and inhalation flow conditions for optimal delivery, and determining bioequivalence between devices. As described in the Introduction, pharmacokinetic testing is one of a number of methods that can be used to investigate inhaler bioequivalence. With pharmacokinetic analysis, systemic drug concentrations are analyzed; however, deposition characteristics in the lung (i.e., the site of action) are not known. It is expected that target sites for specific medicines are distributed unevenly throughout the

lung and deposition at these sites cannot be predicted based on total lung uptake (70,71). Therefore, establishing "lung" bioequivalence requires similar pharmacokinetic profiles as well as verification that deposition characteristics in the lungs are similar between the devices or modes of delivery being considered. A review by Scheuch *et al.* (9) recently highlighted large variability in C/P deposition ratios from imaging studies and showed that C/P cannot be predicted from knowledge of total lung deposition. The lack of correlation between C/P and total lung deposition was attributed to intersubject variability and differences in delivery devices. The CFD model developed in this study can be used to determine C/P ratios for different devices, assuming that the fraction entering the alveolar region is fully deposited. Furthermore, deposition profiles can be predicted within specific regions of the TB airways, as illustrated in Figs. 9, 10, and 11. Therefore, this model may play a valuable role in combination with pharmacokinetic testing to establish bioequivalence between devices. Results of this study indicate that both device and differences in the inhalation profile contribute largely to variability in C/P ratios. Future studies are needed to evaluate the effects of intersubject variability, alveolar deposition characteristics, as well as the time course of drug dissolution and absorption.

Through numerous *in vitro* and *in vivo* studies, certain themes related to the relative performance of MDIs and DPIs have emerged. For the specific inhalers tested, the *in silico* results of this study support these previous findings in some cases and are contradictory in others. Considering the total lung and TB deposition of MDI *vs.* DPI aerosols, previous studies report mixed findings (4,13,14,72). *In vivo* studies reported on the package inserts of both devices tested indicate a nearly identical improvement in FEV_1 for asthmatics already receiving bronchodilators over a 12 week period. However, the shallow dose–response curves of corticosteroids make determining the initial deposition fraction of drug mass impossible. Approximately two times greater total lung deposition was also reported in the *in vivo* study of Hirst *et al.* (14) for an MDI, based on gamma scintigraphy comparisons with two passive DPIs. This result is very consistent with the current study in which the total lung delivery of the MDI (60%) is approximately twice that of the DPI (30%) for correct inhalation profiles.

It is currently held that MDIs are more prone to coordination problems and incorrect usage, which includes incorrect inhalation, than DPIs (6). This is one factor in the increasing development and use of DPIs (4,6). However, results of the current study indicate that the MDI delivers two times more dose to the TB region than the DPI for correct and incorrect usage of each inhaler. Furthermore, both devices showed a similar decrease (~30%) in TB dose associated with incorrect inhalation. The TB dose of the MDI with incorrect inhalation (5.8%) was still 1.4 times higher than the TB dose from the DPI with correct inhalation (4.2%). As a result, both devices appear equally sensitive to the specific errors in inhalation that were considered, and the MDI consistently delivered larger doses to the TB airways, even when it was used incorrectly.

Clearly, the correct inhalation profiles selected for this study are intended to optimize TB deposition. For the corticosteroid considered, MT and alveolar deposition should be minimized and TB deposition should be maximized. Under these criteria, the specified QD and SD inhalation profiles appear most appropriate to maximize TB dose with the DPI and MDI, respectively. Considering targeting deposition to specific regions of the TB airways, results indicate that QD inhalation with both inhalers increases deposition in the range of approximately B4-B7 and SD inhalation increases deposition in approximately B8-B15. A number of studies report that asthma constriction may manifest at different levels of the airways for different individuals and for different triggers (73–75). Results of this study indicate that small increases in regional deposition may be achieved by altering the inhalation profile for both the MDI and DPI. However, these increases appear marginal and are eclipsed by the 2 fold increase in drug deposition associated with the MDI *vs.* DPI. More significantly, the current findings indicate large differences in MT and alveolar deposition between the MDI and DPI. Side effects in the oral airway for patients using a DPI may be improved by switching to an MDI without a decrease in total TB deposition. Conversely, MDI users sensitive to systemic side effects associated with high alveolar deposition may see an improvement in adverse conditions with the use of a DPI.

In contrast with the corticosteroid considered here, inhaled medicines such as proteins and peptides intended for systemic delivery are frequently targeted to the alveolar airways. Considering the delivery platforms evaluated in this study, the MDI delivers nearly half of the initial dose to the alveolar airways with the lowest observed MT deposition. For the DPI, both inhalation profiles deliver an alveolar dose of approximately 26-29%. As a result, the MDI appears to be the preferred platform to maximize alveolar dose with little sensitivity to the inhalation flow rate for the ranges considered.

A limitation of this study is the use of only one incorrect inhalation waveform for each inhaler. Furthermore, only correct *vs.* incorrect inhalation profiles were considered as the source of patient error. O'Callaghan *et al.* (76,77) clearly illustrates a number of patient errors that can occur with MDIs such as inhaling through closed teeth and large inhaler orientation angles. Inhaler errors for both MDIs and DPIs were recently discussed in the review of Smith *et al.* (6). For the MDI, timing of the actuation may be an important factor that was only considered through mean accelerating

flow (i.e., release starting at $t=0$ *vs.* a release time period centered on mean accelerating flow). Actuation at later times, such as during mean decelerating flow may have a more significant impact on deposition than was observed with the cases considered. However, actuation timing variability can be minimized with the use of breath activated MDI and DPI devices. Compared with previous studies, Broeders *et al.* (42) indicated that the correct MDI actuation time is between 0 and 0.2 s and the PIFR should be below 90 L/min. However, in the current study, good performance of the MDI was observed with an actuation time in the range of 0.63–0.83 s for SD and 0.15–0.35 s for QD inhalations. Results of the current study should be interpreted based on the range of inhalation profiles evaluated. Still, the developed models can be used to consider the effects of other activation times, flow rates, waveforms, and geometries.

CONCLUSIONS

In conclusion, the CFD model developed in this study can be used to predict airway deposition characteristics from MDIs and DPIs in order to compare device performance and help establish bioequivalence between devices. For both inhalation profiles considered, the MDI delivered significantly more drug to the TB region and had a similar sensitivity to inhalation errors compared with the DPI. Advantages of MDI delivery included lower MT deposition and improved TB dosing compared with the DPI. The MDI also delivered a large fraction of the initial dose to the alveolar region, under both inhalation profiles, which may be advantageous for systemic absorption. In comparison with the MDI, the main advantage of the DPI was reduced delivery to the alveolar region, which may reduce systemic absorption of topical medications. The dose delivery advantages of the MDI reported in this study should be considered when selecting a platform for respiratory drug delivery to either the TB or alveolar regions of the lungs if the frequently reported limitations, such as timing coordination, can be overcome. To advance the developed CFD model to the point where bioequivalence estimates can be made in conjunction with pharmacokinetic analysis, future studies are needed to assess additional sources of inter- and intra-subject variability, alveolar transport, and drug dissolution and absorption.

ACKNOWLEDGMENTS & DISCLOSURES

This study was supported in part by a contract from the United States Food and Drug Administration (Number HHSF223201000093C). The content is solely the responsibility of the authors and does not necessarily represent the official views of the US Food and Drug Administration.

REFERENCES

1. Byron PR. Drug delivery devices: issues in drug development. Proc Am Thorac Soc. 2004;1:321–8.
2. Finlay WH. The mechanics of inhaled pharmaceutical aerosols. San Diego: Academic; 2001.
3. Newman SP. Principles of metered-dose inhaler design. Respir Care. 2005;50(9):1177–90.
4. Newman SP, Busse WW. Evolution of dry powder inhaler design, formulation, and performance. Respir Med. 2002;96:293–304.
5. Cochrane GM, Bala MV, Downs KE, Mauskopf J, Ben-Joseph RH. Inhaled corticosteroids for asthma therapy: patient compliance, devices, and inhalation technique. Chest. 2000;117:542–50.
6. Smith IJ, Bell J, Bowman N, Everard M, Stein S, Weers JG. Inhaler devices: what remains to be done? J Aerosol Med Pulm Drug Deliv. 2010;23:S25–37.
7. Ross DL, Schultz RK. Effect of inhalation flow rate on the dosing characteristics of dry powder inhaler (DPI) and metered dose inhaler (MDI) products. J Aerosol Med. 1996;9(2):215–26.
8. Tarsin WY, Pearson SB, Assi KH, Chrystyn H. Emitted dose estimates from Seretide Diskus and Symbicort Turbuhaler following inhalation by severe asthmatics. Int J Pharmaceut. 2006;316(1–2):131–7.
9. Scheuch G, Bennett W, Borgstrom L, Clark A, Dalby R, Dolovich M, *et al.* Deposition, Imaging, and Clearance: What Remains to be Done? J Aerosol Med Pulm Drug Deliv. 2010;23:S39–57.
10. Hindle M, Newton DAG, Chrystyn H. Dry powder inhalers are bioequivalent to metered dose inhalers: a study using a new urinary albuterol (salbutamol) assay technique. Chest. 1995;107:629–33.
11. Borgstrom L, Derom E, Stahl E, WahlinBoll E, Pauwels R. The inhalation device influences lung deposition and bronchodilating effect of terbutaline. Am J Respir Crit Care Med. 1996;153(5):1636–40.
12. Bondesson E, Friberg K, Soliman S, Lofdahl CG. Safety and efficacy of a high cumulative dose of salbutamol inhaled via Turbuhaler or via a pressurized metered-dose inhaler in patients with asthma. Respir Med. 1998;92(2):325–30.
13. Bollert FGE, Matusiewicz SP, Dewar MH, Brown GM, McLean A, Greening AP, *et al.* Comparative efficacy and potency of ipratropium via Turbuhaler and pressurized metered-dose inhaler in reversible airflow obstruction. Eur Respir J. 1997;10(8):1824–8.
14. Hirst PH, Bacon RE, Pitcairn GR, Silvasti M, Newman SP. A comparison of the lung deposition of budesonide from Easyhaler, Turbuhaler and pMDI plus spacer in asthmatic patients. Respir Med. 2001;95(9):720–7.
15. Fleming J, Conway J, Majoral C, Tossici-Bolt L, Katz I, Caillibotte G, *et al.* The use of combined single photon emission computed tomography and x-ray computed tomography to assess the fate of inhaled aerosol. J Aerosol Med Pulm Drug Deliv. 2011;24(1):49–60.
16. Longest PW, and Holbrook LT. In silico models of aerosol delivery to the respiratory tract—Development and applications. Advanced Drug Delivery Reviews 2011; doi:10.1016/j.addr.2011.05.009
17. Asgharian B, Hofmann W, Bergmann R. Particle deposition in a multiple-path model of the human lung. Aero Sci Tech. 2001;34:332–9.
18. Kim CS. Deposition of aerosol particles in human lungs: *in vivo* measurement and modeling. Biomarkers. 2009;14(S1):54–8.
19. Martonen TB, Musante CJ, Segal RA, Schroeter JD, Hwang D, Dolovich MA, *et al.* Lung models: strengths and limitations. Respir Care. 2000;45(6):712–36.
20. Ma B, Lutchen KR. CFD simulations of aerosol deposition in an anatomically based human large-medium airway model. Ann Biomed Eng. 2009;37(2):271–85.

21. Lambert AR, O'Shaughnessy PT, Tawhai MH, Hoffman EA, Lin C-L. Regional deposition of particles in an image-based airway model: large-eddy simulation and left-right lung ventilation asymmetry. Aero Sci Tech. 2011;45:11–25.
22. Longest PW, Xi J. Condensational growth may contribute to the enhanced deposition of cigarette smoke particles in the upper respiratory tract. Aero Sci Tech. 2008;42:579–602.
23. Zhang Z, Kleinstreuer C. Computational analysis of airflow and nanoparticle deposition in a combined nasal-oral-tracheobronchial airway model. J Aero Sci. 2011;42:174–94.
24. Kleinstreuer C, Zhang Z. An adjustable triple-bifurcation unit model for air-particle flow simulations in human tracheobronchial airways. J Biomech Eng. 2009;131:021007.
25. Zhang Z, Kleinstreuer C, Kim CS. Comparison of analytical and CFD models with regard to micron particle deposition in a human 16-generation tracheobronchial airway model. Aero Sci. 2009;40:16–28.
26. DeHaan WH, Finlay WH. Predicting extrathoracic deposition from dry powder inhalers. J Aero Sci. 2004;35:309–31.
27. Longest PW, Hindle M, Das Choudhuri S, Xi J. Comparison of ambient and spray aerosol deposition in a standard induction port and more realistic mouth-throat geometry. J Aero Sci. 2008;39:572–91.
28. Longest PW, Hindle M. Quantitative analysis and design of a spray aerosol inhaler. Part 1: Effects of dilution air inlets and flow paths. J Aerosol Med Pulm Drug Deliv. 2009;22(3):271–83.
29. Ilie M, Matida EA, Finlay WH. Asymmetrical aerosol deposition in an idealized mouth with a DPI mouthpiece inlet. Aero Sci Tech. 2008;42:10–7.
30. Longest PW, Hindle M, Das Choudhuri S. Effects of generation time on spray aerosol transport and deposition in models of the mouth-throat geometry. J Aerosol Med Pulm Drug Deliv. 2009;22 (3):67–84.
31. Matida EA, DeHaan WH, Finlay WH, Lange CF. Simulation of particle deposition in an idealized mouth with different small diameter inlets. Aero Sci Tech. 2003;37:924–32.
32. Finlay WH, Martin AR. Modeling of aerosol deposition within interface devices. J Aerosol Med. 2007;20(S1):S19–28.
33. Tian G, Longest PW, Su G, Hindle M. Characterization of respiratory drug delivery with enhanced condensational growth (ECG) using an individual path model of the entire tracheobronchial airways. Ann Biomed Eng. 2011;39(3):1136–53.
34. Tian G, Longest PW, Su G, Walenga RL, Hindle M. Development of a stochastic individual path (SIP) model for predicting the tracheobronchial deposition of pharmaceutical aerosols: effects of transient inhalation and sampling the airways. J Aerosol Sci. 2011;42:781–99.
35. Hindle M, Longest PW. Evaluation of enhanced condensational growth (ECG) for controlled respiratory drug delivery in a mouth-throat and upper tracheobronchial model. Pharm Res. 2010;27:1800–11.
36. Cegla UH. Pressure and inspiratory flow characteristics of dry powder inhalers. Respir Med. 2004;98:S22–8.
37. Swift DL. The oral airway—A conduit or collector for pharmaceutical aerosols. Respiratory Drug Delivery IV 1994:187–195.
38. Fadl A, Wang J, Zhang Z. Metered-dose inhaler efficiency enhancement: A case study and novel design. Inhal Toxicol. 2010;22(7):601–9.
39. Finlay WH, Gehmlich MG. Inertial sizing of aerosol inhaled from two dry powder inhalers with realistic breath patterns *versus* constant flow rates. Int J Pharm. 2000;210:83–95.
40. Byron PR, Delvadia RR, Longest PW, Hindle M. Stepping into the trachea with realistic physical models: uncertainties in regional drug deposition from powder inhalers. Respiratory Drug Delivery. 2010;1:215–24.
41. Delvadia RR, Byron PR, Longest PW, Hindle M. *In vitro* prediction of regional drug deposition from dry powder inhalers. Respiratory Drug Delivery. 2010;2010:907–11.
42. Broeders MEAC, Molema J, Hop WCJ, Folgering HTM. Inhalation profiles in asthmatics and COPD patients: Reproducibility and effect of instruction. J Aerosol Med. 2003;16(2):131–41.
43. Xi J, Longest PW. Transport and deposition of micro-aerosols in realistic and simplified models of the oral airway. Ann Biomed Eng. 2007;35(4):560–81.
44. Cheng KH, Cheng YS, Yeh HC, Swift DL. Measurements of airway dimensions and calculation of mass transfer characteristics of the human oral passage. J Biomech Eng. 1997;119:476–82.
45. Yeh HC, Schum GM. Models of human lung airways and their application to inhaled particle deposition. Bull Math Biology. 1980;42:461–80.
46. ICRP. Human Respiratory Tract Model for Radiological Protection. New York: Elsevier Science Ltd.; 1994.
47. Heistracher T, Hofmann W. Physiologically realistic models of bronchial airway bifurcations. J Aerosol Sci. 1995;26(3):497–509.
48. Horsfield K, Dart G, Olson DE, Cumming G. Models of the human bronchial tree. J Appl Physiol. 1971;31:207–17.
49. Hammersley JR, Olson DE. Physical models of the smaller pulmonary airways. J Appl Physiol. 1992;72:2402–14.
50. Russo J, Robinson R, Oldham MJ. Effects of cartilage rings on airflow and particle deposition in the trachea and main bronchi. Med Eng Phys. 2008;30:581–9.
51. Vinchurkar S, Longest PW. Evaluation of hexahedral, prismatic and hybrid mesh styles for simulating respiratory aerosol dynamics. Computers and Fluids. 2008;37:317–31.
52. Phalen RF, Yeh HC, Schum GM, Raabe OG. Application of an idealized model to morphometry of the mammalian tracheobronchial tree. Anat Rec. 1978;190:167–76.
53. Olsson B, Berg E, Svensson M. Comparing aerosol size distributions that penetrate mouth-throat models under realistic inhalation conditions. Respiratory Drug Delivery. 2010;2010:225–34.
54. van der Palen J. Peak inspiratory flow through Diskus and Turbuhaler, measured by means of a peak inspiratory flow meter (In-Check Dial). Respir Med. 2003;97:285–98.
55. Horsfield K, Dart G, Olson DE, Filley GF, Cumming G. Models of the human bronchial tree. J Appl Physiol. 1971;31:207–17.
56. Asgharian B, Price OT. Airflow distribution in the human lung and its influence on particle deposition. Inhal Toxicol. 2006;18:795–801.
57. Yin Y, Choi J, Hoffman EA, Tawhai MH, Lin C-L. Simulation of pulmonary air flow with a subject-specific boundary condition. J Biomech. 2010;43:2159–63.
58. Hochrainer D, Holz H, Kreher C, Scaffidi L, Spallek M, Wachtel H. Comparison of the aerosol velocity and spray duration of Respimat soft mist inhaler and pressurized metered dose inhalers. J Aerosol Med. 2005;18(3):273–82.
59. Longest PW, Vinchurkar S. Validating CFD predictions of respiratory aerosol deposition: effects of upstream transition and turbulence. J Biomech. 2007;40:305–16.
60. Xi J, Longest PW, Martonen TB. Effects of the laryngeal jet on nano- and microparticle transport and deposition in an approximate model of the upper tracheobronchial airways. J Appl Physiol. 2008;104:1761–77.
61. Longest PW, Hindle M. Das Choudhuri S, and Byron PR. Numerical simulations of capillary aerosol generation: CFD model development and comparisons with experimental data. Aero Sci Tech. 2007;41:952–73.
62. Longest PW, Hindle M. Evaluation of the Respimat Soft Mist inhaler using a concurrent CFD and *in vitro* approach. J Aerosol Med Pulm Drug Deliv. 2009;22(2):99–112.
63. Longest PW, Hindle M, Das Choudhuri S, and Byron PR. Developing a better understanding of spray system design using a combination of CFD modeling and experiment. In: Dalby RN, Byron PR, Peart J, Suman JD, Farr SJ, Young PM editors. Proceedings of Respiratory Drug Delivery 2008. Illinois: Davis Healthcare International Publishing; 2008. p. 151–163.

64. Matida EA, Finlay WH, Grgic LB. Improved numerical simulation of aerosol deposition in an idealized mouth-throat. J Aerosol Sci. 2004;35:1–19.
65. Longest PW, Xi J. Effectiveness of direct Lagrangian tracking models for simulating nanoparticle deposition in the upper airways. Aero Sci Tech. 2007;41:380–97.
66. Stein SW, Myrdal PB. The relative influence of atomization and evaporation on metered dose inhaler drug delivery efficiency. Aero Sci Tech. 2006;40:335–47.
67. Li Z, Kleinstreuer C, Zhang Z. Particle deposition in the human tracheobronchial airways due to transient inspiratory flow patterns. Aerosol Science. 2007;38:625–44.
68. Longest PW, Vinchurkar S. Effects of mesh style and grid convergence on particle deposition in bifurcating airway models with comparisons to experimental data. Med Engr Phys. 2007;29 (3):350–66.
69. Stein SW. Aiming for a moving target: challenges with impactor measurements of MDI aerosols. Int J Pharm. 2008;355 (1–2):53–61.
70. Patton JS, Brain JD, Davies LA, Fiegel J, Gumbleton M, Kim KJ, *et al.* The particle has landed-characterizing the fate of inhaled pharmaceuticals. J Aerosol Med Pulm Drug Deliv. 2010;23:S71–87.
71. Patton JS, Byron PR. Inhaling medicines: delivering drugs to the body through the lungs. Nat Rev Drug Discov. 2007;6:67–74.
72. Warren SJ, Taylor G. Effect of inhalation flow profiles on the deposition of radiolabelled BDP from a novel dry powder inhaler, a conventional metered dose inhaler and MDI plus spacer. In: Dalby RN, Byron PR, Farr SJ, editors. Respiratory Drug Delviery VI. Buffalo Grove: Interpharm Press; 1998. p. 453–5.
73. Anafi RC, Wilson TA. Airway stability and heterogeneity in the constricted lung. J Appl Physiol. 2001;91(3):1185–92.
74. Kotaru C, Coreno A, Skowronski M, Muswick G, Gilkeson RC, McFadden ER. Morphometric changes after thermal and methacholine bronchoprovocations. J Appl Physiol. 2005;98(3):1028–36.
75. Tgavalekos NT, Tawhai M, Harris RS, Mush G, Vidal-Melo M, Venegas JG, *et al.* Identifying airways responsible for heterogeneous ventilation and mechanical dysfunction in asthma: an image functional modeling approach. J Appl Physiol. 2005;99(6):2388–97.
76. O'Callaghan C, Ehtezazi T, Horsfield MA, and Barry PW. A voyage into the respiratory tract. Respiratory Drug Delivery VIII 2002:165–170.
77. O'Callaghan C, Wright P, Shrubb I, and Barry PW. Oral configuration during inhalation from a pressurised metered dose inhaler. Respiratory Drug Delivery VII 2000:589–591.